Three-dimensional failure analysis by BEM using cells with embedded discontinuity activated during the nonlinear loading process

Alisson P. Chaves[1], Rodrigo G. Peixoto[1], Ramon P. Silva[1]

[1]*Universidade Federal de Minas Gerais, Departamento de Engenharia de Estruturas*
Av. Antônio Carlos 6627, Belo Horizonte, CEP 31270-901, Minas Gerais, Brazil
alissonpchaves@ufmg.br, rodrigo.peixoto@dees.ufmg.br, ramon@ufmg.br

Abstract. Numerical simulation of brittle fracture of three-dimensional solids is addressed in this work by the boundary element method (BEM) and the strong discontinuity approach (SDA). In this formulation, cracks are treated using a non-geometric representation through the use of cells with embedded discontinuity. Into these cells, the inelastic strain field is obtained as a result of the application of kinematic equations with discontinuities in the displacement field (strong discontinuities) to standard continuum constitutive models, containing a softening law. A reinterpretation of some parameters of the constitutive model is also performed to guarantee its compatibility to the discontinuous kinematics. Since in the BEM only the internal regions where dissipative effects happen need to be discretized into cells, crack propagation is driven by activations of such cells during the loading process, followed by an expansion of the matrices that define the discrete model.

Keywords: Boundary Element Method, Three-dimensional Nonlinear Analysis, Embedded Discontinuity

1 Introduction

The boundary element method (BEM) has been used for the structural analyses of solids with physically nonlinear behavior since its origins, when it was still known as boundary integral equation method. Following the theory developed by Telles and Carrer [1] which proposes an implicit formulation using the proportional relationship between rates of stress and elastic strain. The initial field increments were written in terms of total strain, resulting in a discrete equilibrium equation, which is linearized and iteratively solved.

In this context, when only elastoplastic constitutive models had been considered, some adaptation were necessary for dealing with quasi-brittle materials. Many effort were dispensed in this subject, as summarized by Peixoto et al.[2]. However, the problems of mesh dependence associated with strain localization and the need for nonlocal strategy for regularization are always present. Fortunately, in the context of the strong discontinuity approach (SDA) the standard continuum constitutive model can be applied even for unbounded strains that are compatible with discontinuous displacement field (Oliver [3]).

Manzoli and Venturini [4, 5] works introduced discontinuity interfaces inside triangular cells that dicretize the whole domain. They used associative elastoplastic constitutive models with a specific yield criterion, together with an exponential softening law to represent the behavior of crack in quasi-brittle materials. Later, this idea was extended by using an isotropic damage model and a tracking algorithm to generate cells automatically, in the direction of the crack path determined during the analyses (Manzoli et al. [6]). A further improvement was presented by Peixoto et al. [7, 8], who sophisticated the nonlinear analysis, involving inelastic dissipation with softening in continuous media, bifurcation analysis and transition between weak and strong discontinuities. They used subparametric quadrilateral cells with constant approach (uniform displacement jumps) with another automatic cells generation algorithm. In a subsequent work, Mendonça et al. [9] successfully proposed the use of non-uniform displacement jumps inside a cell to overcome the stress locking phenomena reported in [7, 8].

This work presents some steps for the extension of SDA modeling with BEM for three-dimensional failure analyses, considering that all aforementioned works which used this formulation were limited to two-dimensional problems. Here, the implicit BEM formulation is used for the analysis of solids with physically nonlinear behavior, under monotonic load and small deformations. An elastic-degrading constitutive model with an exponential

softening law for isotropic materials are considered together with the SDA. In particular, the strong discontinuity regime is imposed directly after the end of the elastic regime with the discontinuity surface defined as perpendicular to the maximum principal stress. This is a typical behavior of material failure in isotropic brittle materials. Quadrilateral linear isoparametric boundary elements are used together with hexahedral constant cells with embedded discontinuity that were placed aligned along the crack surface. The implementations were performed at the collaborative open source system INSANE (INteractive Structural ANalysis Environment) [10].

2 Strong discontinuity approach

The incorporation of strong discontinuity approach in the standard integral equations requires some adaptation. Its development starts with the consideration of a solid (domain Ω, boundary Γ), with a discontinuity surface $\mathcal{S}$ (unit normal vector $\mathbf{n}$), surrounded by an arbitrary sub-domain $\Omega_\varphi \subset \Omega$, as represented in Fig. 1.

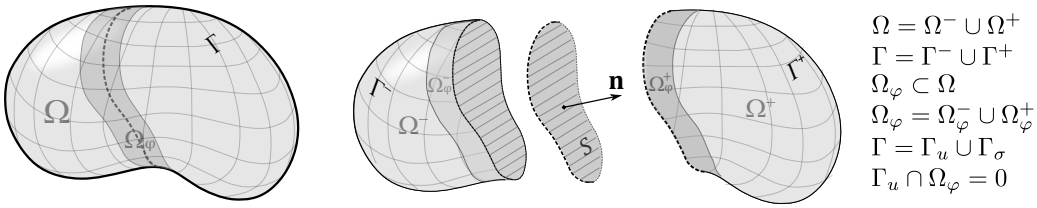

Figure 1. Solid with discontinuity surface $\mathcal{S}$ in an arbitrary sub-domain Ω_φ

For a material point $\mathbf{X}$, an arbitrary function $\varphi(\mathbf{X})$ is defined in Ω_φ (see section 5.1), with $\varphi(\mathbf{X}) = 0$ in $\Omega^-\backslash\Omega^-_\varphi$ and $\varphi(\mathbf{X}) = 1$ in $\Omega^+\backslash\Omega^+_\varphi$. At a given instant, when the strong discontinuity is completely developed, the displacement and the total strain field can be described, together with the well known Heaviside function ($\mathcal{H}$), by the regularized expression detailed in [7, 8] as follows:

$$u_i(\mathbf{X},t) = \underbrace{\bar{u}_i(\mathbf{X},t) + \varphi(\mathbf{X})[\![u_i]\!](\mathbf{X},t)}_{\hat{u}_i(\mathbf{X},t)} + \underbrace{\big[\mathcal{H}_\mathcal{S}(\mathbf{X}) - \varphi(\mathbf{X})\big]}_{\mathcal{M}^\varphi_\mathcal{S}(\mathbf{X})}[\![u_i]\!](\mathbf{X},t) = \hat{u}_i(\mathbf{X},t) + \mathcal{M}^\varphi_\mathcal{S}(\mathbf{X})[\![u_i]\!](\mathbf{X},t) \quad (1)$$

$$\epsilon_{ij}(\mathbf{X},t) = \underbrace{\frac{1}{2}(\hat{u}_{i,j} + \hat{u}_{j,i})}_{\hat{\epsilon}_{ij}} + \underbrace{\frac{\mathcal{M}^\varphi_\mathcal{S}}{2}([\![u_{i,j}]\!] + [\![u_{j,i}]\!]) - \frac{1}{2}(\varphi_{,i}[\![u_j]\!] + \varphi_{,j}[\![u_i]\!])}_{-\epsilon^\varphi_{ij}} + \frac{\delta_\mathcal{S}}{2}\big([\![u_i]\!]n_j + [\![u_j]\!]n_i\big) \quad (2)$$

where $\bar{u}_i(\mathbf{X},t)$ is the regular part of the displacement field, $[\![u_i]\!](\mathbf{X},t)$ is the displacement jump component on the discontinuity surface, and $\hat{u}_i(\mathbf{X},t)$ represents a continuous function. Complementing, $\mathcal{M}^\varphi_\mathcal{S}(\mathbf{X})$ takes zero value everywhere in Ω, except in Ω_φ. Also, $\hat{\epsilon}_{ij}$ is the regular strain and ϵ^φ_{ij} has null value outside the sub-domain Ω_φ. Finally, the last term in eq. 2 is restricted to the discontinuity surface, where n_j are components of its unitary normal vector, and $\delta_\mathcal{S}$ represents the Dirac delta function over $\mathcal{S}$.

For the continuity condition of the traction vector at the discontinuity interface, for a given instant of time, the following equation must be satisfied for points at the discontinuity surface:

$$f_i(\hat{\epsilon}_{ij}, [\![u_i]\!], [\![u_{i,j}]\!]) = \big\{E^o_{ijkl}\big[\hat{\epsilon}_{kl} - \epsilon^\varphi_{kl}([\![u_i]\!], [\![u_{i,j}]\!])\big] - \sigma^\mathcal{S}_{ij}(\epsilon_{ij})\big\}n_j = 0 \quad (3)$$

where $\sigma^\mathcal{S}_{ij}$ represents stress components on $\mathcal{S}$, and E^o_{ijkl} corresponds to the constitutive linear elastic tensor.

The domain have to be discretized only where the discontinuity is supposed to occur, i.e., the subdomain Ω_φ. Inside each cell with embedded discontinuity, each component ϵ^φ_{ij} is a function of the displacement jump components $[\![u_i]\!]$ only, once they can be assumed to be constant inside each cell. Thus, for a given regular strain $\hat{\epsilon}_{ij}$, $f_i \equiv f_i([\![u_i]\!]) = 0$. These components can be evaluated iteratively through the linearisation of eq. (3). Then, for a given $[\![u_i]\!](\hat{\epsilon}_{ij})$ achieved from the solution of eq. (3), a constitutive regularized equation can be obtained, as follows:

$$\tilde{\sigma}_{ij}(\hat{\epsilon}_{ij}) = \sigma^{\Omega\backslash\mathcal{S}}_{ij}\big(\hat{\epsilon}_{ij} - \epsilon^\varphi_{ij}([\![u_i]\!])\big) = E^o_{ijkl}(\hat{\epsilon}_{kl} - \epsilon^\varphi_{kl}) \quad (4)$$

3 Implicit BEM formulation

Three boundary integral equations: the Somigliana's identity for displacements at internal points, the displacement boundary integral equation and the integral equation for internal strains, can be rewritten with the discontinuity terms. Once natural and essential boundary conditions are applied at the discretized boundary, those three equations can be rearranged in the following discrete equations:

$$\{\dot{u}^{\Omega}\} = [A^u]\{\dot{x}\} + [B^u]\{\dot{y}\} + [Q^u_{\epsilon^\varphi}]\{\dot{\epsilon}^\varphi\} \tag{5}$$

$$[A]\{\dot{x}\} = [B]\{\dot{y}\} + [Q_{\epsilon^\varphi}]\{\dot{\epsilon}^\varphi\} \tag{6}$$

$$\{\dot{\hat{\epsilon}}\} = [A^\epsilon]\{\dot{x}\} + [B^\epsilon]\{\dot{y}\} + [Q^\epsilon_{\epsilon^\varphi}]\{\dot{\epsilon}^\varphi\} \tag{7}$$

where $\{\dot{x}\}$ and $\{\dot{y}\}$ are, respectively, the boundary unknowns and the prescribed values of displacement $\dot{\hat{u}}_i$ or traction $\dot{t}_i$, while $\{\dot{u}^{\Omega}\}$ and $\{\dot{\hat{\epsilon}}\}$ are relative to internal collocation points. The term $\{\dot{\epsilon}^\varphi\}$ represents the inelastic strain components and matrices referenced by $[A]$, $[B]$ contain the integrals over the boundary elements, adding the free term c_{ij} where appropriate. Matrices $[Q]$ hold the integrals over internal cells, adding, conveniently, the free terms $F^{\epsilon\epsilon}_{ijkl}$ (which arise when the integral equation for internal strains is obtained) into $[Q^\epsilon_{\epsilon^\varphi}]$.

Following the implicit BEM procedure, eq. (6) can be solved for $\{\dot{x}\}$ and substituted into eq. (7), giving:

$$\{\dot{\hat{\epsilon}}\} = [N^\epsilon]\{\dot{y}\} + [M^\epsilon_{\epsilon^\varphi}]\{\dot{\epsilon}^\varphi\}; \text{ with: } [N^\epsilon] = [A^\epsilon][A^{-1}][B] + [B^\epsilon] \text{ and } [M^\epsilon_{\epsilon^\varphi}] = [A^\epsilon][A^{-1}][Q_{\epsilon^\varphi}] + [Q^\epsilon_{\epsilon^\varphi}] \tag{8}$$

Regarding the rate independent constitutive damage model considered in this work, time evolution of non-linear analysis can be considered as finite incremental differences. Hence, for the *i-th* increment, eq. (8) turns:

$$\{\hat{\epsilon}\}^i = \lambda^i[N^\epsilon]\{y\} + [M^\epsilon_{\epsilon^\varphi}]\{\epsilon^\varphi\}^i \tag{9}$$

where the load factor λ^i is a cumulative scalar value for load increment, defined by the control method employed.

In a given step i, an equilibrium (or residual) vector $\{Q\}^i$ can be defined as a function of the regular strains and the load factor $\{Q(\hat{\epsilon}^i, \lambda^i)\}^i$ as follows:

$$\{Q\}^i = \lambda^i[N^\epsilon]\{y\} + [M^\epsilon_{\epsilon^\varphi}]\big(\{\epsilon\}^i - [E^o]^{-1}\{\tilde{\sigma}(\hat{\epsilon})\}^i\big) - \{\hat{\epsilon}\}^i \tag{10}$$

where $[E^o]$ represents the linear elastic constitutive relationship matrix and $\{\tilde{\sigma}(\hat{\epsilon})\}$ is the stress vector, obtained from the regular strains, as stated in eq. (4): the regularized constitutive equation.

The equilibrium condition set in eq. (10) has to be verified at each load increment. This can be performed numerically through the Newton-Raphson's method. A detailed description of this incremental-iterative solution strategy, and the control method employed can be seen in [2].

4 Interface constitutive model

An isotropic damage constitutive model is used here to represent damage dissipation in finite regions of a solid domain, over the discontinuity surface. The usual expressions for this model are summarized in many references (*e.g.* Oliver et al. [11] and refs. [7–9]). The set of expressions encompasses: free energy, constitutive equation, damage variable, internal variable evolution law, damage criterion, loading-unloading conditions and softening law.

Regarding the relationship between stress and strain rates, it is given through a constitutive tangent tensor E^t_{ijkl}, which is equal to E_{ijkl} for unloading (or neutral load). Thus:

$$\dot{\sigma}^{\mathcal{S}}_{ij} = E^t_{ijkl}\dot{\epsilon}_{kl} = E_{ijkl}\dot{\epsilon}_{kl} + \dot{E}_{ijkl}\epsilon_{kl}\ ; \text{ where } E^t_{ijkl} = E_{ijkl} - \left(\frac{\partial D}{\partial r}\right)\left(\frac{\partial \tau_\epsilon}{\partial \epsilon_{kl}}\right)E^o_{ijrs}\epsilon_{rs} \tag{11}$$

with r representing the strain-like scalar internal variable, and D the damage variable. For the equivalent strain τ_ϵ this work used the expression presented in [11], i.e., $\tau_\epsilon = \sqrt{\epsilon^+_{ij}E^o_{ijkl}\epsilon_{kl}}$, in which, the tensor $\epsilon^+_{ij} = \sum_{k=1}^{3}(\langle\epsilon_k\rangle\hat{\mathbf{e}}_k\otimes\hat{\mathbf{e}}_k)$ is defined in a coordinate system aligned with the principal strain directions: ϵ_k represents the k-th principal strain, $\hat{\mathbf{e}}_k$ is the unit vector in the corresponding principal direction, and $\langle\cdot\rangle$ refers to the Macaulay brackets. Complementing, the exponential softening law for the strong discontinuity regime, used here, was presented in [6].

5 Numerical implementation features

The analysis of solids by BEM requires the discretization of its boundary into elements, where the displacements and tractions are approximated. This work considers the use of isoparametric quadrilateral boundary elements, with linear function assumed for the variation of the known (and unknown) boundary values and the boundary shape.

Hexahedral cells with constant function, compatible with uniform displacement jump inside the cell (see eq. 2), are used in this work. One functional node is placed at the centroid of each cell (collocation point ξ^c). Each cell has the geometry parametrized by conventional linear shape functions (M^α), and its geometrical vertex nodes (α), Fig. 2a. For each cell, regular integrals are performed through standard Gauss quadrature, based on the criterion presented by Eberwien et al. [12]. Integrals with weakly singular kernels are evaluated through the techniques presented by Lachat and Watson [13]. For strongly singular integrals the technique proposed by Gao and Davies [14] is applied.

5.1 Cells with embedded discontinuity

Strong discontinuity dissipative effects are restricted to the sub-domain Ω_φ, which needs dicretization. For constant cells, the field ϵ_{ij}^{φ} has only one value inside each cell, *i.e.*, $\epsilon_{ij}^{\varphi} \approx \epsilon^{\varphi,c}$ for $\mathbf{X} \in \Omega_c$. The discontinuity surface inside a cell is, therefore, described by one plane with a unitary vector normal ($\mathbf{n}$) defining its orientation (see Fig. 2c). A very small scalar parameter, h, is used to regularize the Dirac delta function.

The function $\varphi(\mathbf{X})$ inside a cell can be expressed from the usual geometric parametrization functions (M^α), as they are defined by values one or zero at nodes. The summation is taken over the interpolation functions associated to the geometric vertices located at Ω_c^+ side of the cell (see Fig. 2c).

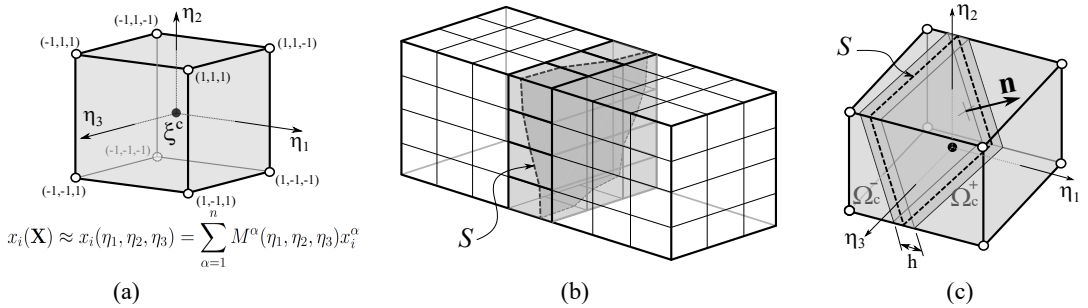

(a) (b) (c)

Figure 2. Domain discretization: (a) Hexahedral cell in natural coordinates η_i, geometric nodes (○) and functional node (●); (b) example of boundary and domain discretization; (c) cell with embedded discontinuity.

5.2 Displacement jumps

Inside each cell, the displacement jump components on the discontinuity surface are considered constants, *i.e.*, $[\![u_i]\!](\mathbf{X}) \approx [\![u^c]\!]$ for $\mathbf{X} \in \Omega_c$. These values are obtained from the numerical solution of eq. (3). For this purpose, the inelastic strains at a point inside a cell ($\epsilon^{\varphi,c}$) can be written in terms of the displacement jump as:

$$\{\epsilon^{\varphi,c}\} = [\nabla^s \varphi]\{[\![u^c]\!]\} \tag{12}$$

The iterative method of Newton-Raphson is employed for the solution of eq. (3), in a given particular state of regular strain, $\{\hat{\epsilon}^c\}$. Its linearised form is given by:

$$\{f\}_{j-1} + [\bar{N}^c]^T \left[-[E^o][\nabla^s\varphi] - \left[\frac{\partial \sigma^{\mathcal{S}}}{\partial \epsilon}\right]_{j-1} \left[\frac{1}{h}[N^c] - [\nabla^s\varphi]\right]\right]\{\delta[\![u^c]\!]\}_j \approx \{0\} \tag{13}$$

where $[E^o]$ corresponds to the constitutive linear elastic tensor E^o_{ijkl}, the parameter h is a very small scalar used to regularize the Dirac delta function (and appears in the constitutive model softening law), j is an iterative index, and the term $\left[\frac{\partial \sigma^{\mathcal{S}}}{\partial \epsilon}\right]$ is the matrix form of the tangent operator of the constitutive model used to represent the dissipative effects over the discontinuity surface $\mathcal{S}$, given in eq. (11). Furthermore, expressions for $[\bar{N}^c]^T$, $[N^c]$ and the terms in $[\nabla^s\varphi]$ are:

$$\varphi_{,i} = \frac{\partial \varphi}{\partial \eta_k}\frac{\partial \eta_k}{\partial X_i} = \left(\frac{\partial M^\alpha}{\partial \eta_k} X_i^\alpha\right)^{-1}\left(\frac{\partial}{\partial \eta_k}\left[\sum_{\alpha^+} M^{\alpha^+}\right]\right) \tag{14}$$

$$[\bar{N}^c]^T = \begin{bmatrix} n_1 & 0 & 0 & n_2 & n_3 & 0 \\ 0 & n_2 & 0 & n_1 & 0 & n_3 \\ 0 & 0 & n_3 & 0 & n_1 & n_2 \end{bmatrix}; \quad [N^c] = \begin{bmatrix} n_1 & 0 & 0 & \frac{1}{2}n_2 & \frac{1}{2}n_3 & 0 \\ 0 & n_2 & 0 & \frac{1}{2}n_1 & 0 & \frac{1}{2}n_3 \\ 0 & 0 & n_3 & 0 & \frac{1}{2}n_1 & \frac{1}{2}n_2 \end{bmatrix}^T \tag{15}$$

5.3 Regularized constitutive model in a cell

The nonlinear procedure to evaluate the displacement jump is performed inside each cell with embedded discontinuity, every iteration during the solution of eq. (10), in order to update the regularized stress, $\{\tilde{\sigma}\}$, given by eq. (4). Thus, it is convenient to present here the discrete version of eq. (4) in a cell, i.e.,

$$\{\tilde{\sigma}(\hat{\epsilon}^c)\} = [E^o](\{\hat{\epsilon}^c\} - \{\epsilon^{\varphi,c}\}) = [E^o](\{\hat{\epsilon}^c\} - [\nabla^s\varphi^c]\{[\![u]\!]\}) \tag{16}$$

Moreover, the tangent operator associated to this regularized constitutive model, is also required for the nonlinear solution of the equilibrium condition vector, eq. (10), and can be obtained after differentiation of eq. (16).

6 Activation of cells during the process

The internal region where dissipative effects happen has to be discretized into cells. These cells are part of the discrete model, and its respective vectors refereed to displacement rate, strain rate and initial fields, are all associated to internal points. Such vectors can be present in the matrix systems since the first step of the nonlinear analysis, or they can be added gradually during the loading process, according to the activation of the cells. The use of progressive activation allows the use of the current approach coupled with a tracking path algorithm to determine, during the process, the position of new cells, as done in [6–9] for two-dimensional problems.

For the gradual activation, some vectors have to be expanded, by introducing the respective subvectors relative to the new added cell: $\{\dot{\hat{u}}^{\Omega}_{N}\}$, $\{\dot{\hat{\epsilon}}_{N}\}$ and $\{\dot{\epsilon}^{\varphi}_{N}\}$. Then eqs. (5), (6) and (7) become:

$$\left\{\begin{array}{c}\dot{\hat{u}}^{\Omega}\\ \hline \dot{\hat{u}}^{\Omega}_{N}\end{array}\right\} = \left[\begin{array}{c}A^{u}\\ \hline a^{u}\end{array}\right]\{\dot{x}\} + \left[\begin{array}{c}B^{u}\\ \hline b^{u}\end{array}\right]\{\dot{y}\} + \left[\begin{array}{c|c}Q^{u}_{\epsilon^{\varphi}} & q^{u}_{C}\\ \hline q^{u}_{R} & q^{u}_{RC}\end{array}\right]\left\{\begin{array}{c}\dot{\epsilon}^{\varphi}\\ \hline \dot{\epsilon}^{\varphi}_{N}\end{array}\right\} \tag{17}$$

$$[A]\{\dot{x}\} = [B]\{\dot{y}\} + \left[\begin{array}{c|c} Q_{\epsilon^{\varphi}} & q_{\epsilon^{\varphi}}\end{array}\right]\left\{\begin{array}{c}\dot{\epsilon}^{\varphi}\\ \hline \dot{\epsilon}^{\varphi}_{N}\end{array}\right\} \tag{18}$$

$$\left\{\begin{array}{c}\dot{\hat{\epsilon}}\\ \hline \dot{\hat{\epsilon}}_{N}\end{array}\right\} = \left[\begin{array}{c}A^{\epsilon}\\ \hline a^{\epsilon}\end{array}\right]\{\dot{x}\} + \left[\begin{array}{c}B^{\epsilon}\\ \hline b^{\epsilon}\end{array}\right]\{\dot{y}\} + \left[\begin{array}{c|c}Q^{\epsilon}_{\epsilon^{\varphi}} & q^{\epsilon}_{C}\\ \hline q^{\epsilon}_{R} & q^{\epsilon}_{RC}\end{array}\right]\left\{\begin{array}{c}\dot{\epsilon}^{\varphi}\\ \hline \dot{\epsilon}^{\varphi}_{N}\end{array}\right\} \tag{19}$$

where the coefficients of the new submatrices have to be evaluated using different source points and regions of integration: $[q_{\epsilon^{\varphi}}]$ are evaluated considering source point at boundary; $[q^{u}_{C}]$ and $[q^{\epsilon}_{C}]$ are evaluated considering source point at existent internal points; $[q^{u}_{R}]$, $[q^{\epsilon}_{R}]$, $[q^{u}_{RC}]$, $[q^{\epsilon}_{RC}]$, $[a^{u}]$, $[b^{u}]$, $[a^{\epsilon}]$ and $[b^{\epsilon}]$ are evaluated considering the added source (internal) points. For the coefficients $[a^{u}]$, $[b^{u}]$, $[a^{\epsilon}]$, $[b^{\epsilon}]$ integrations are performed in the boundary elements; for the coefficients $[q^{u}_{R}]$, $[q^{\epsilon}_{R}]$ integrations are performed in the existent cells; and for the coefficients $[q_{\epsilon^{\varphi}}]$, $[q^{u}_{C}]$, $[q^{\epsilon}_{C}]$, $[q^{u}_{RC}]$, $[q^{\epsilon}_{RC}]$ integrations are performed in the added cell.

The matrices in eq. (8) also have to be expanded, as follows:

$$\left[\begin{array}{c}N^{\epsilon}\\ \hline n^{\epsilon}\end{array}\right] = \left[\begin{array}{c}A^{\epsilon}\\ \hline a^{\epsilon}\end{array}\right][A]^{-1}[B] + \left[\begin{array}{c}B^{\epsilon}\\ \hline b^{\epsilon}\end{array}\right] \;\Rightarrow\; [n^{\epsilon}] = [a^{\epsilon}][A]^{-1}[B] + [b^{\epsilon}] \tag{20}$$

$$\left[\begin{array}{c|c}M^{\epsilon}_{\epsilon^{\varphi}} & m^{\epsilon}_{C}\\ \hline m^{\epsilon}_{R} & m^{\epsilon}_{RC}\end{array}\right] = \left[\begin{array}{c}A^{\epsilon}\\ \hline a^{\epsilon}\end{array}\right][A]^{-1}\left[\begin{array}{c|c} Q_{\epsilon^{\varphi}} & q_{\epsilon^{\varphi}}\end{array}\right] + \left[\begin{array}{c|c}Q^{\epsilon}_{\epsilon^{\varphi}} & q^{\epsilon}_{C}\\ \hline q^{\epsilon}_{R} & q^{\epsilon}_{RC}\end{array}\right] \tag{21}$$

with: $[m^{\epsilon}_{C}] = [A^{\epsilon}][A]^{-1}[q_{\epsilon^{\varphi}}] + [q^{\epsilon}_{C}]$; $[m^{\epsilon}_{R}] = [a^{\epsilon}][A]^{-1}[Q_{\epsilon^{\varphi}}] + [q^{\epsilon}_{R}]$; $[m^{\epsilon}_{RC}] = [a^{\epsilon}][A]^{-1}[q_{\epsilon^{\varphi}}] + [q^{\epsilon}_{RC}]$.

Some more similar expansion of matrices are needed, from the equations arisen from handling eq. (5) and eq. (6). It is worth to mention, that the existent coefficients from all these matrices do not need to be recalculated. The new submatrices are just added accordingly, by augmenting rows and columns of the existent matrices.

7 Numerical simulation

This example presents the analysis of a bar under simple tension, with a circular corner notch. Dimensions and material properties are presented in Fig. 3a. The failure surface is supposed to occur at the horizontal notch plane highlighted. Hexahedral cells with embedded discontinuity were applied for the discretization of this region of the solid. Exponential damage evolution was considered for dissipation effects. The control method adopted to drive the incremental-iterative procedure is the direct displacement, with a convergence tolerance for eq. (10) fixed as 1×10^{-4}. An assumed value of 0.01mm was adopted for the parameter h in eq. (13).

Three meshes, with different refinements, were considered as shown in Fig. 3b (only cells are shown). Displacement control of corner point A (Fig. 3a) was adopted for the nonlinear analysis progress. Results for the displacement equilibrium path of point A and an intermediate point B are plotted at Fig. 4. A theoretical reference value for critical fracture stress $\sigma_{f\text{crit}}$ is also shown in Fig. 4. It was calculated as a particular case of the stress-intensity solution for a quarter-elliptical corner crack, given by Anderson [15].

The peak stress achieved in the equilibrium path converges to a value a little bellow the reference theoretical critical fracture stress. The increase in mesh refinement provides a good representation of the unload behavior. Also, from the results for point B (not a control node) it is possible to note a typical snap-back of the equilibrium path. The gradual activation of discontinuity at the cells on the fracture plane, in different load steps is schematically presented in Fig. 5.

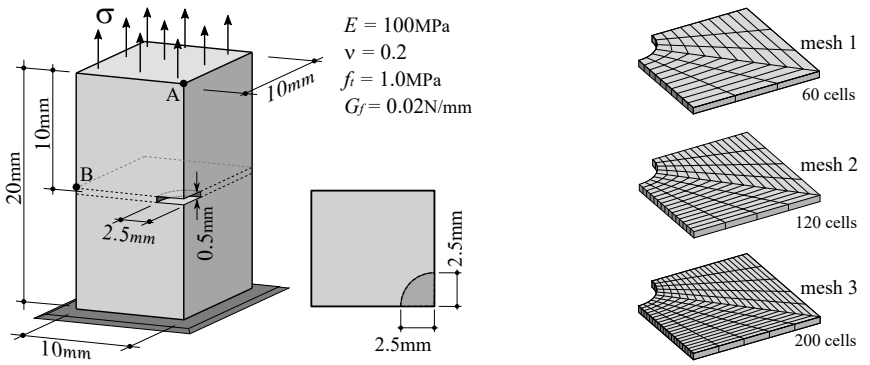

Figure 3. Prismatic bar under simple tension, with a circular corner notch: (a) dimensions and material properties; (b) meshes for internal discretization

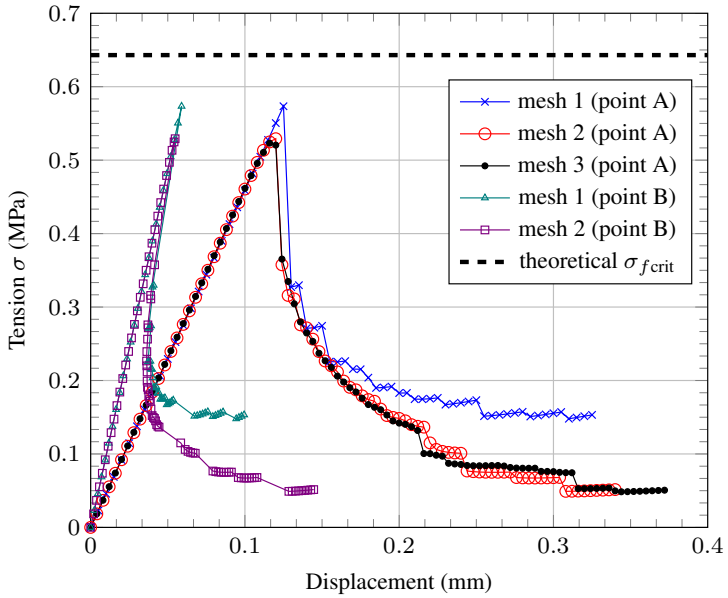

Figure 4. Displacement equilibrium path for control point A, for point B, and the theoretical reference.

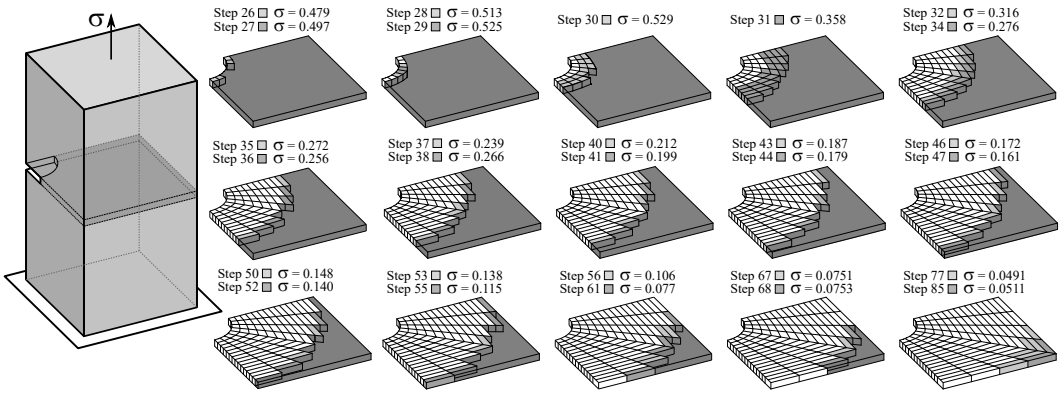

Figure 5. Gradual activation of discontinuity at the notch plane (mesh 2)

8 Conclusions

This work presented some aspects of the usage of implicit formulation of the BEM associated with the strong discontinuity and a damage constitutive model for three-dimensional analysis of solids. The numerical example showed the capability of the implemented algorithm to describe the equilibrium path in a typical fracture mechanics

problem. A progressive activation of discontinuity inside the cells was observed, according to the evolution of stress values in the domain. Despite the simple example, this is an important aspect for the analysis of crack propagation in solids. The potential of the approach allows its sophistication through the implementation of a tracking algorithm for automatic generation of cells in the domain, in order to reproduce a crack path. All these stages of evolution has already been successfully developed for bi-dimensional analysis, but are still in course for three-dimensional problems.

Acknowledgements. The authors gratefully acknowledge the financial support received from the Brazilian agency of research funding: CNPq - Conselho Nacional de Desenvolvimento Científico e Tecnológico (Grant number 432471/2018-9).

Authorship statement. The authors hereby confirm that they are the sole liable persons responsible for the authorship of this work, and that all material that has been herein included as part of the present paper is either the property (and authorship) of the authors, or has the permission of the owners to be included here.

References

[1] J. C. F. Telles and J. A. M. Carrer. Implicit procedures for the solution of elastoplastic problems by the boundary element method. *Mathematical and Computer Modelling*, vol. 15, pp. 303–311, 1991.
[2] R. G. Peixoto, F. E. S. Anacleto, G. O. Ribeiro, R. L. S. Pitangueira, and S. S. Penna. A solution strategy for non-linear implicit BEM formulation using a unified constitutive medelling framework. *Engineering Analysis with Boundary Elements*, vol. 64, pp. 295–310, 2016.
[3] J. Oliver. Modelling strong discontinuities in solid mechanics via softening constitutive equations. Part 1: Fundamentals. *International Journal for Numerical Methods in Engineering*, vol. 39, pp. 3575–3600, 1996.
[4] O. L. Manzoli and W. S. Venturini. Uma formulação do MEC para simulação numérica de descontinuidades fortes. *Revista Internacional de Métodos Numéricos para Cálculo y Diseño en Ingeniería*, vol. 20, n. 3, pp. 215–234, 2004.
[5] O. L. Manzoli and W. S. Venturini. An implicit BEM formulation to model strong discontinuities. *Computational Mechanics*, vol. 40, pp. 901–909, 2007.
[6] O. L. Manzoli, R. A. Pedrini, and W. S. Venturini. Strong discontinuity analysis in solid mechanics using boundary element method. In E. J. Sapountzakis and M. H. Aliabadi, eds, *Advances in Boundary Element Techniques X - Proceedings of the 10th International Conference (BETEQ 2009)*, pp. 323–329, Athens, Greece, 2009.
[7] R. G. Peixoto, G. O. Ribeiro, R. L. S. Pitangueira, and S. S. Penna. The strong discontinuity approach as a limit case of strain localization in the implicit bem formulation. *Engineering Analysis with Boundary Elements*, vol. 80, pp. 127–141, 2017.
[8] R. G. Peixoto, G. O. Ribeiro, and R. L. S. Pitangueira. A boundary element method formulation for quasi-brittle material fracture analysis using the continuum strong discontinuity approach. *Engineering Fracture Mechanics*, vol. 202, pp. 47–74, 2018.
[9] T. S. Mendonça, R. G. Peixoto, and G. O. Ribeiro. A new class of cells with embedded discontinuity for fracture analysis by the boundary element method. *International Journal for Numerical Methods in Engineering*, vol. 121, pp. 3869–3892, 2020.
[10] INSANE Project. Interactive structural analysis environment, development code available at the Git repository: http://git.insane.dees.ufmg.br/insane/insane.git , information on the project: https://www.insane.dees.ufmg.br/en/home/, (2021).
[11] J. Oliver, A. E. Huespe, S. Blanco, and D. L. Linero. Stability and robustness issues in numerical modeling of material failure with the strong discontinuity approach. *Computer Methods in Applied Mechanics and Engineering*, vol. 195, pp. 7093–7114, 2006.
[12] U. Eberwien, C. Duenser, and W. Moser. Efficient calculation of internal results in 2D elasticity bem. *Engineering Analysis with Boundary Elements*, vol. 29, pp. 447–453, 2005.
[13] J. C. Lachat and J. O. Watson. Effective numerical treatment of boundary integral equations – A formulation for three dimensional elastostatics. *International Journal for Numerical Methods in Engineering*, vol. 10, pp. 991–1005, 1976.
[14] X.-W. Gao and T. G. Davies. An effective boundary element algorithm for 2D and 3D elastoplastic problems. *International Journal of Solids and Structures*, vol. 37, pp. 4987–5008, 2000.
[15] T. L. Anderson. *Fracture Mechanics – Fundamentals and applications*. Taylor & Francis Group, third edition, 2005.